

Hilde Lea Lein · Øystein Skottun Andersen ·
Per Erik Vullum · Edgar Lara-Curzio ·
Randi Holmestad · Mari-Ann Einarsrud · Tor Grande

Mechanical properties of mixed conducting $\text{La}_{0.5}\text{Sr}_{0.5}\text{Fe}_{1-x}\text{Co}_x\text{O}_{3-\delta}$ ($0 \leq x \leq 1$) materials

Received: 23 December 2005 / Accepted: 9 January 2006 / Published online: 21 April 2006
© Springer-Verlag 2006

Abstract Young's modulus, strain–stress behavior, fracture strength, and fracture toughness of $\text{La}_{0.5}\text{Sr}_{0.5}\text{Fe}_{1-x}\text{Co}_x\text{O}_{3-\delta}$ ($0 \leq x \leq 1$) materials have been investigated in the temperature range 20–1,000 °C. Young's moduli of $\text{La}_{0.5}\text{Sr}_{0.5}\text{Fe}_{0.5}\text{Co}_{0.5}\text{O}_{3-\delta}$ and $\text{La}_{0.5}\text{Sr}_{0.5}\text{CoO}_{3-\delta}$, measured by resonant ultrasound spectroscopy, were 130 ± 1 and 133 ± 3 GPa, respectively. The nonlinear stress–strain relationship observed by four-point bending at room temperature was inferred as a signature of ferroelastic behavior of the materials. Above the ferroelastic to paraelastic transition temperature, the materials showed elastic behavior, but due to high-temperature creep, a nonelastic response reappeared above ~ 800 °C. The room temperature fracture strength measured by four-point bending was in the range 107–128 MPa. The corresponding fracture toughness of $\text{La}_{0.5}\text{Sr}_{0.5}\text{Fe}_{0.5}\text{Co}_{0.5}\text{O}_{3-\delta}$, measured by single edge V-notch beam method, was 1.16 ± 0.12 MPa·m^{1/2}. The measured fracture strength and fracture toughness were observed to increase with increasing temperature. The fracture mode changed from intragranular at low temperature to intergranular at high temperature. Tensile stress gradient at the surface of the materials caused by a frozen-in gradient in the oxygen content during cooling was proposed to explain the low ambient temperature fracture strength and toughness.

Keywords Mixed conductors · Oxygen permeable membranes · Perovskites · Mechanical properties

Introduction

Sr-substituted $\text{LaFe}_{1-x}\text{Co}_x\text{O}_{3-\delta}$ materials are candidates for oxygen permeable membranes, gas sensors, and electrodes in high-temperature electrochemical devices due to their high electronic and ionic conductivity at elevated temperatures [1–6]. One of the main challenges for these applications is to prevent mechanical failure during fabrication and during operation of devices. The knowledge of mechanical properties of these materials is therefore essential, particularly at the high temperature due to desired long lifetime of devices and estimation of reliability. The fracture strength and fracture toughness of alkali-earth-substituted LaMO_3 (M=La, Co, Mn, Cr, Ga) perovskite materials, relevant for these technologies, have been reported the last two decades, but only a few studies report on the mechanical properties at high temperature. The room temperature fracture strength of LaMO_3 (M=La, Co, Mn, Cr, Ga)-based materials, measured by four-point bending, is typically 100–160 MPa [7–11]. The corresponding fracture toughness of the materials is reported in the range 1.3–2.8 MPa·m^{1/2} [7, 8, 12, 13], where orthorhombic perovskites have higher fracture toughness than rhombohedral and cubic perovskites. The fracture strength of rhombohedral and cubic materials generally decreases with increasing temperature [8, 11, 14]. The fracture toughness is either constant or decreasing with increasing temperature [8, 12, 13]. There are conflicting reports on the Young's modulus of these materials. The Young's modulus in the range 100–200 GPa has been reported, but there is no physical explanation for the large variation. Different methods have however been applied, but when data from the most reliable techniques [15] are considered, the Young's modulus of LaMO_3 materials is in the range 120–200 GPa [10, 12, 16, 17].

Rhombohedral $\text{La}_{0.5}\text{Sr}_{0.5}\text{Fe}_{1-x}\text{Co}_x\text{O}_{3-\delta}$ transform to cubic perovskites around 300 °C [18]. The thermal

H. L. Lein · Ø. S. Andersen · M.-A. Einarsrud · T. Grande (✉)
Department of Materials Science and Engineering,
Norwegian University of Science and Technology,
7491 Trondheim, Norway
e-mail: Grande@material.ntnu.no
Tel.: +47-73-594084
Fax: +47-73-590860

P. E. Vullum · R. Holmestad
Department of Physics,
Norwegian University of Science and Technology,
7491 Trondheim, Norway

E. Lara-Curzio
High Temperature Materials Laboratory,
Oak Ridge National Laboratory,
Oak Ridge, TN 37831, USA

expansions of $\text{La}_{0.5}\text{Sr}_{0.5}\text{Fe}_{1-x}\text{Co}_x\text{O}_{3-\delta}$ between ambient temperature and $1,000^\circ\text{C}$ are 1.5–2.3% in air and 1.7–2.5% in N_2 atmosphere. The considerable expansion is due to chemical expansion as the oxygen deficiency, $3-\delta$, decreases from 2.93–2.97 to 2.78–2.84 in air or 2.66–2.77 in N_2 in the same temperature region [18].

Recently, it has been shown that rhombohedral and orthorhombic perovskite materials have ferroelastic behavior resulting in hysteresis in the stress–strain relationship [7, 11, 13, 19, 20]. $\text{La}_{0.5}\text{Sr}_{0.5}\text{Fe}_{1-x}\text{Co}_x\text{O}_{3-\delta}$ materials are expected to be ferroelastic below the cubic to rhombohedral phase transition, and twinning below the phase transition is expected leading to ferroelastic domains which can be reoriented by external stress [21]. The reorientation of the ferroelastic domains under mechanical stress may lead to toughening of the materials, and the temperature dependence of the fracture toughness of rhombohedral and orthorhombic perovskites has been related to ferroelasticity [7, 13]. In the paraelastic phase, no domains are present and the materials are elastic.

$\text{La}_{0.5}\text{Sr}_{0.5}\text{Fe}_{1-x}\text{Co}_x\text{O}_{3-\delta}$ and related materials show low creep resistance at elevated temperatures [22–23] (Lein et al., unpublished data). Creep rates in the range $1 \cdot 10^{-9}$ – $2 \cdot 10^{-8} \text{ s}^{-1}$ are reported at 900°C for $x=0.5$ and $x=1$, and even larger creep rates in inert atmosphere (Lein et al., unpublished data). Stress during operation will therefore lead to creep in these materials, and creep may also give rise to systematic errors in four-point bending experiments as shown in this paper.

Here, we report on Young's modulus, strain–stress behavior, ferroelasticity, fracture strength, and fracture toughness of $\text{La}_{0.5}\text{Sr}_{0.5}\text{Fe}_{1-x}\text{Co}_x\text{O}_{3-\delta}$ materials. Particular attention is devoted to the observed temperature variation of the measured mechanical properties.

Experimental

Materials preparation

$\text{La}_{0.5}\text{Sr}_{0.5}\text{Fe}_{1-x}\text{Co}_x\text{O}_{3-\delta}$ [$x=0.5$ (LSFC), 0.75 (LSF25C75), and 1 (LSC)] powders were synthesized by spray drying of glycine/nitrate solutions as described elsewhere [18]. Calcined powders were uniaxially pressed (60 MPa) into bars ($8 \times 8 \times 58$ mm, for four-point bending) or cylinders [diameter 10 mm and length 20 mm, for resonant ultrasound spectroscopy (RUS)], and finally pressed isostatically at 200 MPa. The relative green densities obtained were 52–54% of theoretical densities. The samples were sintered in air at $1,150^\circ\text{C}$ for 2 h (LSFC1, LSF25C75) or 12 h (LSFC2, LSC). The heating rate was $200^\circ\text{C}/\text{h}$. To avoid cracking during cooling, the cooling rate was $50^\circ\text{C}/\text{h}$ ($1,150$ – 750°C), $6^\circ\text{C}/\text{h}$ (750 – 450°C), and $100^\circ\text{C}/\text{h}$ (450°C –room temperature).

Bars for mechanical testing were machined (Mil. Spec. 1942) to $3 \times 4 \times 45 \text{ mm}^3$. All the edges were chamfered. After machining, some of the bars were annealed at 500°C for 2 h to eliminate possible preferential orientation of ferroelastic domains caused by the machining. The end faces of the cylinders were ground and polished (until

diamond size of $1 \mu\text{m}$) for determination of Young's modulus.

Characterization of microstructure and phase composition

The microstructure of the materials before and after the mechanical testing was investigated with a Hitachi S3500N scanning electron microscope (SEM) and a JEOL 2010F transmission electron microscope (TEM) equipped with a field emission gun (FEG), operating at 200 kV. The grain sizes were estimated by a linear intercept method from SEM images of polished ($1\text{-}\mu\text{m}$ diamond finish) and thermally etched (0.2 h, $1,130^\circ\text{C}$) surfaces. Ten images were taken from different parts of the polished samples. To verify the phase purity, X-ray powder diffraction (XRD) of calcined powders and sintered materials were performed on a Siemens D 5005 θ – θ diffractometer using CuK radiation. Thermogravimetry (TG) was performed using a heating rate of $2\text{K}/\text{min}$ on the crushed sintered samples using a Netzsch STA 449C instrument up to $1,100^\circ\text{C}$. Dilatometry (DIL) was performed on sintered samples using a Netzsch DIL 402C instrument up to $1,000^\circ\text{C}$.

Characterization of mechanical properties

Four-point bending strength of machined specimens was measured at different temperatures between room temperature and $1,000^\circ\text{C}$ using a fully articulating 40/20 span SiC bend fixture (MTS Model 642.85). Deflection of the specimens during loading was measured with a MTS Model 632.70-03 Bend Bar Extensometer with three extensometer pushrods (Model 602.81). The two outer pushrods were placed in correspondence with the two upper rollers of the bend fixture, whereas the third was placed in the center of the sample. A total of 5–11 bars were tested for each temperature. Fracture toughness (K_{IC}) was measured by the single edge notch beam (SENB) method or single edge V-notch beam (SEVNB) method at different temperatures using the same fixture as described above. The notch depths of the SENB specimen were ~ 0.8 or 1.2 mm, and the widths were ~ 0.2 mm. For the SEVNB specimen, the notches were machined to 0.8 mm and further cut with a razor blade to total to 0.9 – 1.0 mm to make a V-notch. The fracture toughness was calculated using equations from ISO 15732 [24, 25]. A total of 3–4 bars were tested at each temperature. The mechanical testing was performed by using a Cormet 20-kN electro-mechanical machine with a 2-kN HBM load cell and a Sigmatest-controlled atmosphere furnace with a Kanthal A heating element and nickel radiation shields. The heating rate was $200^\circ\text{C}/\text{h}$, whereas the cooling rate was $300^\circ\text{C}/\text{h}$. The furnace chamber was evacuated and backfilled with synthetic air before the high-temperature measurements, and the measurements were performed in flowing synthetic air. The bars were equilibrated at the measurement temperature for 1 h before the measurements. For the

high-temperature measurements, the samples were exposed to a load of 14 MPa during heating to avoid any movements in the fixture during the heating. The measurements were performed in position control with rates of 8 $\mu\text{m/s}$ for four-point bending and 1 $\mu\text{m/s}$ for SENB and SEVNB measurements. The dimensions of the specimens were corrected for thermal expansion [18]. One of the LSF25C75 bars was kept at 800 °C at constant stress (25 MPa) for 18 h, and the creep rate in the steady-state region at the end of the relaxation was calculated. The fracture surfaces were examined by SEM to determine the fracture origins.

Selected LSFC2 samples were also heat treated in flowing N_2 ($p_{\text{O}_2} \sim 10^{-4}$ atm) at 800 or 1,000 °C to prepare samples for measurement of fracture strength and fracture toughness at elevated temperature in N_2 . Heating and cooling rates in the ranges 15–100 and 50–100 °C/h, respectively, were tried. Due to extended fracture of the bars, only two bars were tested for fracture strength at room temperature.

The Young's modulus of the LSFC and LSF materials was measured by RUS. Cylinders were placed on the top of three piezoelectric transducers, and further placed in a resistance-heated furnace with controlled atmosphere. Measurements were performed for each sample in the 50- to 400-Hz frequency range with a resolution of 0.035 Hz. A multidimensional algorithm (Quasar International) was used to analyze the spectra by fitting the obtained frequency peaks to theoretical peaks based on dimensions, density, and a set of guessed elastic constants. New elastic constants were then calculated. Young's modulus for the materials was obtained for every 100 °C from room temperature up to 1,200 °C in air and N_2 atmospheres ($p_{\text{O}_2} \sim 10^{-4}$ atm).

Results and discussion

Microstructure and phase composition

The relative density, average grain size, and excess Co_3O_4 content in the materials are given in Table 1. The theoretical densities used for the calculation of theoretical density were 6.29 g cm^{-3} (LSFC), 6.30 g cm^{-3} (LSF25C75), and 6.42 g cm^{-3} (LSC) calculated from X-ray diffractograms and oxygen nonstoichiometry [18]. The influence of secondary phases was neglected in the calculation of theoretical densities.

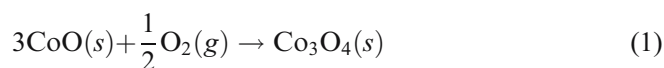
A typical image of the microstructure of these materials is shown in Fig. 1a. The pores in the materials were submicron in size as seen in the insert in Fig. 1a. Larger flaws observed as the fracture origins did also contribute to the closed porosity.

Thermogravimetric analysis showed that small amounts of Co_3O_4 were present in the materials (Table 1), indicating a small deviation from nominal composition. The excess Co-oxide was located in separate grains about 0.5 μm in size and consisting of several Co_3O_4 crystallites as shown in the TEM image in Fig. 1b. The Co_3O_4 crystallites were formed according to reaction (1)

Table 1 Relative density, average grain size and excess Co_3O_4 content for the $\text{La}_{0.5}\text{Sr}_{0.5}\text{Fe}_{1-x}\text{Co}_x\text{O}_{3-\delta}$ materials sintered at different temperatures

Composition	Label	Sintering time at 1,150 °C (h)	Relative density (%)	Grain size (μm)	Co_3O_4 content (wt%)
0.5	LSFC1	2	97	0.8±0.1	0.10
0.5	LSFC2	12	95	1.1±0.2	0.99
0.75	LSF25C75	2	97	1.4±0.3	2.8
1	LSC1	12	99	1.7±0.4	0.39
1	LSC2	12	99	1.7±0.4	0.98

when excess CoO was oxidized to Co_3O_4 during cooling of the material from the sintering temperature.



The expansion due to reaction (1) is 16.4 vol%, which introduces compressive “radial” stresses and tensile hoop stresses in the perovskite matrix surrounding the Co_3O_4

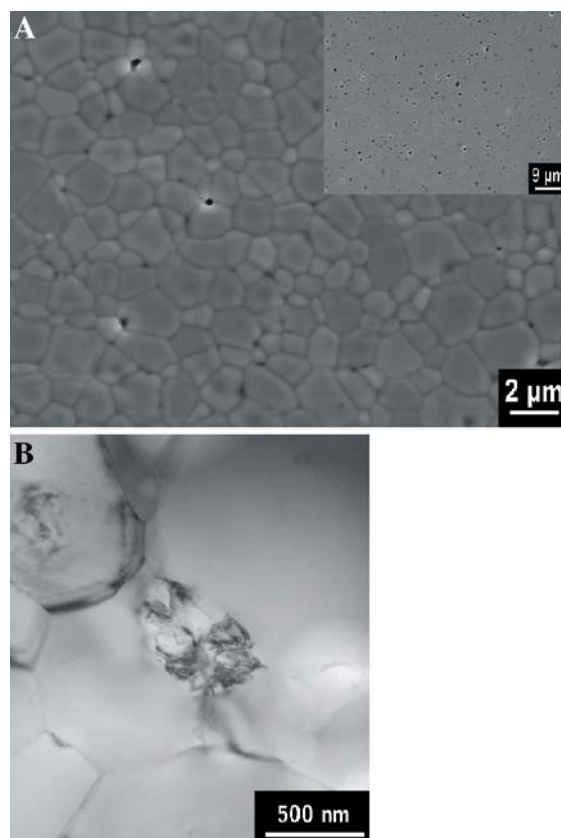


Fig. 1 a Scanning electron microscope (SEM) image of etched surface of $\text{La}_{0.5}\text{Sr}_{0.5}\text{Fe}_{0.5}\text{Co}_{0.5}\text{O}_{3-\delta}$ material sintered at 1,150 °C for 12 h (LSFC2). *Inset*: Polished surface of the same material. b TEM image of $\text{La}_{0.5}\text{Sr}_{0.5}\text{Fe}_{0.5}\text{Co}_{0.5}\text{O}_{3-\delta}$ (LSFC1) with an inclusion consisting of several Co_3O_4 crystallites

inclusions. For LSF25C75 containing 2.8 wt% Co_3O_4 , the expansion was observed by DIL between 950 and 910 °C to be 0.3 vol%. For the other materials, the effect of the Co_3O_4 inclusions was not detectable by DIL. The stresses generated around the Co_3O_4 inclusions due to the volume expansion may result in crack deflection and enhancement of the fracture toughness [26].

Young's modulus

The Young's modulus of the LSFC2 and LSC2 materials measured by RUS in air and N_2 is shown as a function of temperature in Fig. 2. The average value of the Young's moduli for LSFC and LSC for $T < 400$ °C are 130 ± 1 and 133 ± 3 GPa, respectively, independent on atmosphere. Generally, Young's modulus of polycrystalline ceramics, without grain boundary softening, is expected to decrease about 1% per hundred Kelvin [26]. Two of the data sets demonstrate a depression of the Young's modulus with increasing temperature. The temperature dependence of Young's modulus can also generally be described by Eq. (2) according to Hillig [27–29]

$$\frac{E}{E_0} = 1 - \left(\frac{T}{T_m} \right)^3 \quad (2)$$

where E_0 is the Young's modulus at room temperature, T is the actual temperature, and T_m is the melting temperature of the material. The model is compared to the measured data in Fig. 2 using $E_0 = 131$ GPa and the melting point of LaFeO_3 [30] (dashed line) and SrFeO_3 [31, 32] (solid line). The model predicts a considerably sharper reduction of the Young's modulus with increasing temperature than observed. The thermal and chemical expansion of the materials [18] is thus not significantly influencing the

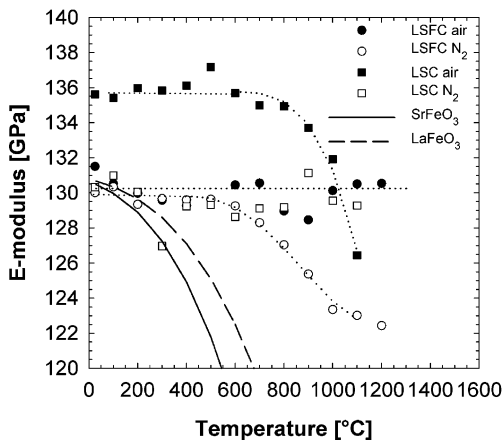


Fig. 2 Young's modulus of $\text{La}_{0.5}\text{Sr}_{0.5}\text{Fe}_{0.5}\text{Co}_{0.5}\text{O}_{3-\delta}$ (LSFC2) and $\text{La}_{0.5}\text{Sr}_{0.5}\text{Co}_{0.5}\text{O}_{3-\delta}$ (LSC2) in air and N_2 atmosphere as a function of temperature, measured by resonant ultrasound spectroscopy. The solid and the dashed lines represent the model from Hillig [27–29], and the dotted lines are guides to the eye

Young's modulus. Contribution from frozen-in tensional stresses at the surface as discussed further below is also not effecting the Young's modulus. The Young's modulus of the materials is therefore considered close to constant in the whole temperature range studied. The minor reduction of the Young's modulus above ~ 600 °C might be related to the onset of creep (Lein et al., unpublished data) in this temperature region.

Strain–stress relationship and apparent Young's modulus

The strain–stress relationship for LSFC2 and LSF25C75 at different temperatures measured by four-point bending is given in Figs. 3 and 4. LSC1 investigated at room temperature and 800 °C showed a similar behavior as LSF25C75. At room temperature, the strain–stress relationship is nonlinear, and for LSFC2, an inflection point around 80 ± 10 MPa is observed (Fig. 3). This nonlinear behavior is interpreted as the signature of ferroelasticity because it corresponds to a part of a hysteresis in the strain–stress relationship [7, 13]. For LSF25C75 and LSC, the inflection point in strain–stress behavior is at a higher stress level than the maximum stress level at fracture. The strain–stress data observed at room temperature demonstrate that the present materials are ferroelastic. At 400 °C and higher temperatures, the stress–strain relationship does not show any inflection point, which is expected because the materials transform to the paraelastic phase above 300 °C [18]. A linear stress–strain behavior is expected for the paraelastic state.

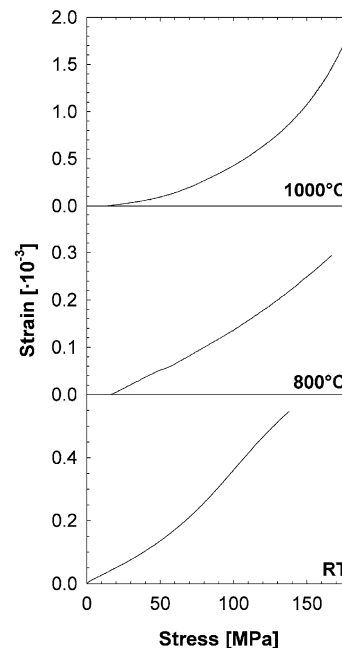
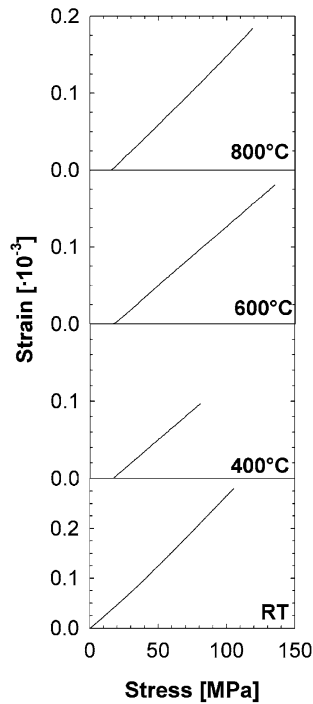


Fig. 3 Strain vs stress relationship for $\text{La}_{0.5}\text{Sr}_{0.5}\text{Fe}_{0.5}\text{Co}_{0.5}\text{O}_{3-\delta}$ (LSFC2) at room temperature, 800, and 1,000 °C. Note that for measurements at elevated temperature, a prestress of 14 MPa was applied to the sample during heating

Fig. 4 Strain vs stress relationship for $\text{La}_{0.5}\text{Sr}_{0.5}\text{Fe}_{0.25}\text{Co}_{0.75}\text{O}_{3-\delta}$ (LSF25C75) at room temperature, 400, 600, and 800 °C. Note that for measurements at elevated temperature, a prestress of 14 MPa was applied to the sample during heating



Pronounced nonlinear stress–strain behavior reappeared at high temperatures, especially at 1,000 °C. The nonlinear response at high temperature was due to creep. The steady-state tensional creep rate of LSF25C75 at 800 °C and 25 MPa measured by four-point bending was $6.8 \times 10^{-10} \text{ s}^{-1}$. This creep rate is in reasonable agreement with the creep rates observed for LSFC2 under compression (Lein et al., unpublished data). These significant creep rates at 800 °C and above are therefore responsible for the observed nonelastic strain–stress behavior at high temperature.

The Young's modulus is proportional to the inverse slope of strain vs stress for elastic materials with symmetric deformation of the four-point bending bars. The apparent Young's modulus obtained from strain–stress relationships of the present materials is summarized in Table 2. The apparent Young's modulus is calculated using the inverse slope of the strain measured up to 5- to 10-MPa stress. The apparent Young's modulus given in Table 2 is not in good agreement with the Young's modulus obtained by RUS. Particularly, the temperature dependence of the apparent Young's modulus determined by four-point bending is nonphysical as the Young's modulus should decrease with increasing temperature [26]. The increasing apparent Young's modulus from room temperature to 400 °C and above is most likely related to the ferroelastic behavior of the materials below 300 °C. At high temperatures and high stresses, where creep contributed to the stress–strain relationship, a systematic depression of the apparent Young's modulus is expected. At low stress levels, the creep is not considered to affect the stress–strain relationship, and we, therefore, have no reliable explanation for the nonphysical behavior of the apparent Young's modulus calculated from four-point bending. The overall conclusion is that the Young's modulus of the materials obtained by

Table 2 Apparent Young's modulus and fracture strength of $\text{La}_{0.5}\text{Sr}_{0.5}\text{Fe}_{1-x}\text{Co}_x\text{O}_{3-\delta}$ materials at different temperatures measured by four-point bending

Composition	Temperature (°C)	Apparent Young's modulus (GPa)	Fracture strength (MPa)	Number of bars
LSFC1	RT, nonannealed	115±5	107±15	11
	RT, annealed	116±10	121±7	5
	800	160±10	181±13	5
LSFC2	RT, annealed	118±7	128±12	8
	800	169±8	166±15	6
	1,000	121±11	181±23	5
LSF25C75	RT, annealed	115±3	71±7	6
	400, annealed	176±8	61±20	3
	600	177±4	121±11	3
	800	160±10	120±11	5
LSC1	RT, nonannealed	122±5	138±12	8
	800	157±7	181±18	6

The given uncertainty is the standard deviation between the different bars

RT Room temperature

RUS is the far most credible data obtained, and that Young's modulus obtained by four-point bending may suffer large systematic errors due to nonelastic behavior due to ferroelastic behavior or creep.

Fracture strength

The fracture strength of the materials obtained by four-point bending is included in Table 2. This fracture strength is the linear-elastically computed strength for all data, even in the cases where a nonlinear behavior was observed. The calculated fracture strength is unrealistically high when nonlinear strain–stress relationship is observed due to the nonsymmetric deformation of the test bar on the tensional and compressional side [33, 34]. We have not performed any analysis of the magnitude of this systematic error leading to a too high calculated strength.

Machining of the bars before the mechanical testing may induce preferential orientation of the ferroelastic domains due to the stresses applied. This preferential orientation of domains may reduce the fracture strength. Here, it is seen that heat treatment at 500 °C for 2 h gives a small increase in the fracture strength for LSFC1 at room temperature from 107±15 to 121±7 MPa, and a decrease in standard deviation is observed. These results show that the bars should be heat treated before measurements at temperatures below the ferroelastic to paraelastic phase transition temperature in accordance with previous reports [13]. Above the phase transition temperature, the ferroelastic domains will disappear and heat treatment before the measurements is not considered to be necessary.

The fracture origins of all samples were porous regions or flaws with extension up to ~100 μm. In a few cases, a

secondary phase due to impurities (not Co_3O_4 inclusions) was observed as the fracture origin. The fracture mirrors were also easily seen, especially for the fracture surfaces of bars tested at room temperature. An example of a porous fracture origin and fracture mirror of LSFC1 is shown in Fig. 5. At room temperature and 400°C , an intragranular fracture mode was generally observed, whereas at temperatures above 600°C , an intergranular fracture mode was observed as can be seen from the fracture surfaces of LSFC2 at room temperature and 800°C given in Fig. 6.

The fracture strength increased with increasing temperature (see Table 2). Several factors contribute to the uncertainty of the calculated strength, and these are discussed in the following. Deviation from linear and symmetrical deformation will lead to systematic errors in the calculated fracture strength. Because the deviation from linear deformation is largest at temperatures below 300°C (due to ferroelasticity) and at the high temperatures (due to creep), a minimum in calculated fracture strength is expected at around $400\text{--}600^\circ\text{C}$ where the materials were elastic. Because such a minimum in calculated fracture strength was not observed (Table 2), the nonelastic behavior and error related to this are not the major factors giving the increase in fracture strength with increasing temperature. The effect of the Co_3O_4 secondary phase is not expected to significantly affect the fracture strength, except a small negative effect due to reduction of Co_3O_4 . The loss of the ferroelastic behavior at the ferroelastic to paraelastic phase transition temperature will also cause a reduction in the fracture strength of the materials. The change from transgranular to intergranular fracture mode with increasing temperature may contribute to the observed increase in nominal fracture strength, but we have observed similar change in fracture mode in other materials without a significant change in the strength [13].

The factor which we believe is the most significant for the observed increase in fracture strength with increasing

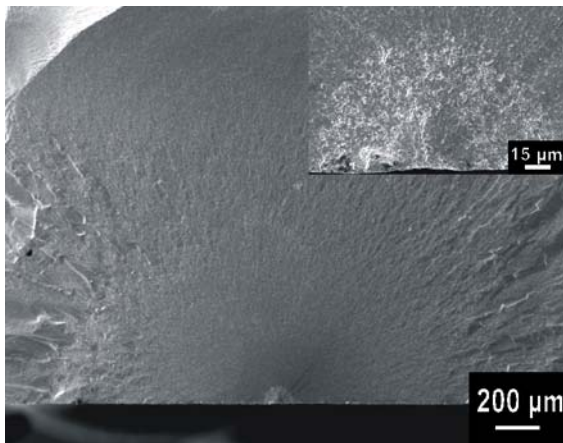


Fig. 5 SEM image of a fracture surface after four-point bending of a $\text{La}_{0.5}\text{Sr}_{0.5}\text{Fe}_{0.5}\text{Co}_{0.5}\text{O}_{3-\delta}$ (LSFC1) bar. The fracture mirror is easily seen. The *inset* is the fracture origin

temperature is the frozen-in gradient in oxygen content at the surface. A gradient in oxygen content was generated during cooling of the materials from the sintering temperature. Due to kinetics of the oxidation and diffusion of oxygen ions, the interior of the bars was less oxidized compared to the surface. Due to the chemical contraction upon oxidation, tensile stresses on the surface of the test bars will occur. The stress gradients generated will lead to a lower strength of the materials below the temperature where the oxidation process was frozen in. During testing at elevated temperatures, where the oxygen diffusivity becomes sufficient for equilibration of the oxygen content, the oxygen gradient will be eliminated, and hence, a higher fracture strength value was obtained at these temperatures. We therefore suggest that fracture strength observed at elevated temperatures is more representative for the fracture strength of stress-free materials than the fracture strength obtained at room temperature. The significant effect of the stress gradients is supported by a very large fraction of bars cracked when these test bars were exposed to N_2 atmosphere.

Based on DIL of polycrystals [18], the oxygen content of the bulk is frozen in at $400\text{--}600^\circ\text{C}$. The oxygen loss and chemical expansion are considerably higher in N_2 . Stresses in membranes induced by the gradient in δ are conveniently normalized with respect to the magnitude of the maximum possible biaxial stress, σ_{max} , expressed as [35]

$$|\sigma_{\text{max}}| = \hat{E} \left| \varepsilon_{c,\text{max}} \right| \quad (3)$$

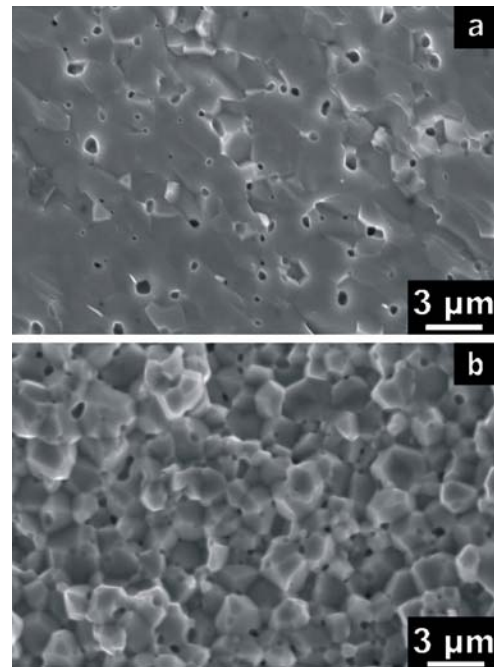


Fig. 6 SEM images of a fracture surface of $\text{La}_{0.5}\text{Sr}_{0.5}\text{Fe}_{0.5}\text{Co}_{0.5}\text{O}_{3-\delta}$ (LSFC2) after four-point bending measurements at (a) room temperature and (b) 800°C

Table 3 Fracture toughness measured by single edge notch beam (SENB) method and by single edge V-notch beam (SEVNB) method for $\text{La}_{0.5}\text{Sr}_{0.5}\text{Fe}_{1-x}\text{Co}_x\text{O}_{3-\delta}$ materials at different temperatures

Composition	Method	Notch length (mm)	Temperature (°C)	Fracture toughness ($\text{MPa}\cdot\text{m}^{1/2}$)	Number of bars
LSFC1	SENB	0.75–0.78	RT, nonannealed	1.31 ± 0.11	3
		1.14–1.16	RT, nonannealed	1.84 ± 0.33	3
LSFC2	SEVNB	0.87–0.96	RT, annealed	1.16 ± 0.12	5
		0.92–0.95	800	1.48 ± 0.16	5
		0.92–0.95	1,000	2.26 ± 0.20	4
LSC1	SENB	1.17–1.20	RT, nonannealed	1.47 ± 0.44	3
		1.16–1.19	RT, annealed	1.49 ± 0.30	3
		1.16–1.18	800	2.88 ± 0.44	3

where $\varepsilon_{c,\max}$ is the maximum chemical strain, and \hat{E} is related to the Young's modulus, E , and the Poisson's ratio, ν , by

$$\hat{E} = \frac{E}{1 - \nu} \quad (4)$$

$\varepsilon_{c,\max}$ is calculated to 9×10^{-4} at a fracture stress of 166 MPa using a Young's modulus of 130 GPa (LSFC2) and Poisson's ratio of 0.33. The chemical expansion, ε_c , found for LSFC at 800 °C between air and N_2 atmosphere was 4.5×10^{-3} [18]. A frozen-in strain in the order of the chemical stress will therefore lead to fracture or crack growth from surface flaw of the same size found as the fracture origin in the materials. Tensile stress due to chemical contraction at the surface or difference in oxidation state between bulk and surface may give stresses in the order of the critical stress for crack initiation and

crack propagation. Similar effects on the mechanical properties have also been reported for Sr-substituted LaMnO_3 [17].

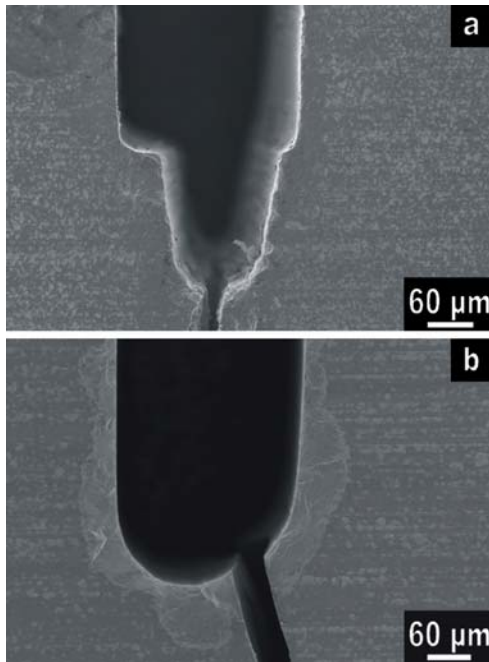
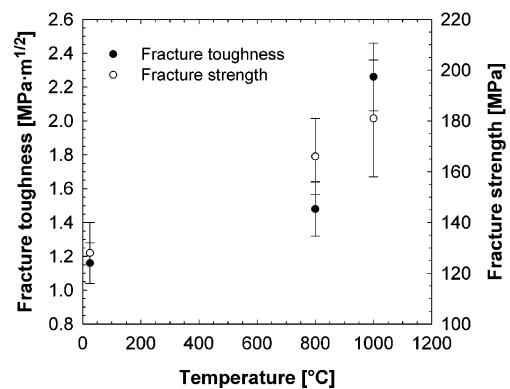
Fracture toughness

Fracture toughness of the materials obtained by SENB and SEVNB methods are summarized in Table 3. The annealing of the LSC bars did not influence the absolute values of the toughness. The standard deviation for the measurements performed by the SEVNB method is smaller compared with that by the SENB method due to the better-defined notch as illustrated in Fig. 7.

The measured fracture toughness increased with increasing temperature. Both the fracture toughness and the fracture strength show the same temperature dependency, as shown in Fig. 8, which is in accordance with Eq. (3) [26]

$$\sigma_f = K_{IC} / Yc^{1/2} \quad (5)$$

where Y is a dimensionless factor dependent on the crack configuration, and c is the half of the crack length or the entire length of an edge crack. The stress gradient developed due to the difference in oxygen stoichiometry is therefore also influencing the fracture toughness.

**Fig. 7** Notch shape for (a) a SEVNB bar (LSFC2) and (b) a SENB bar (LSC1) of $\text{La}_{0.5}\text{Sr}_{0.5}\text{Fe}_{0.5}\text{Co}_{0.5}\text{O}_{3-\delta}$ materials**Fig. 8** Fracture strength and fracture toughness of $\text{La}_{0.5}\text{Sr}_{0.5}\text{Fe}_{0.5}\text{Co}_{0.5}\text{O}_{3-\delta}$ as a function temperature

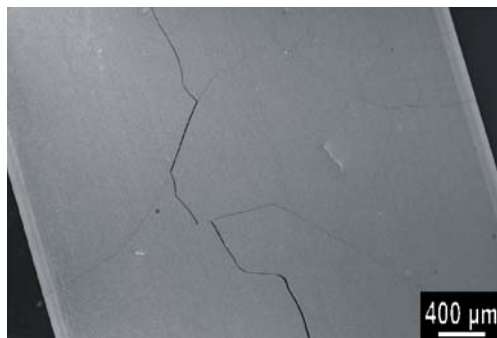


Fig. 9 Surface of a $\text{La}_{0.5}\text{Sr}_{0.5}\text{Fe}_{0.5}\text{Co}_{0.5}\text{O}_{3-\delta}$ bar (LSFC2) heat treated in N_2 atmosphere before fracture strength measurement

Fracture strength of bars annealed in N_2 atmosphere

The measured fracture strengths of two LSFC2 bars annealed in nitrogen atmosphere were 13 and 24 MPa. After heat treatment in N_2 atmosphere, the surface of the samples appeared cracked as can be seen from Fig. 9. The large surface cracks resulted in the low fracture strength. A large fraction of the samples did also fracture during the heat treatment in N_2 atmosphere, showing that considerable stress gradients develop in the materials due to gradient in oxygen concentration or valance of Co. This is also in agreement with the proposed effect of the stresses due to oxygen concentration gradient on the nominal fracture strength of the materials.

Conclusion

A nonlinear ferroelastic strain–stress relationship was observed for $\text{La}_{0.5}\text{Sr}_{0.5}\text{Fe}_{1-x}\text{Co}_x\text{O}_{3-\delta}$ materials, $0.5 \leq x \leq 1$, below the ferroelastic to paraelastic phase transition, whereas a linear relationship was observed above the transition until creep resulted in plastic deformation. The room temperature fracture strength and fracture toughness were 107–128 MPa and $1.16\text{--}1.84 \text{ MPa}\cdot\text{m}^{1/2}$, respectively, and both the strength and the toughness were observed to increase with increasing temperature. The improvement of the mechanical properties with increasing temperature was attributed to relaxation of the frozen-in stress gradients at the surface of the materials during cooling. Young's moduli of $\text{La}_{0.5}\text{Sr}_{0.5}\text{Fe}_{0.5}\text{Co}_{0.5}\text{O}_{3-\delta}$ and $\text{La}_{0.5}\text{Sr}_{0.5}\text{CoO}_{3-\delta}$, measured by RUS, were 130 ± 1 and 133 ± 3 GPa, respectively. Apparent Young's modulus, calculated from strain–stress relationship, was not in good agreement with the data obtained by RUS. The present findings have demonstrated the importance of understanding ferroelasticity, chemically induced stresses, and creep in order to understand the mechanical properties of mixed valence state rhombohedral perovskite materials.

Acknowledgements The Research Council of Norway, Statoil, and Hydro are acknowledged for financial support. A special thanks to Miladin Radovic for help in performing the RUS measurements.

References

- Bouwmeester H MJ, Burgaaf AJ (1997) Dense ceramic membranes for oxygen separation. In: Gellings PJ, Bouwmeester H MJ (ed) The CRC handbook of solid state electrochemistry. CRC Press, Inc., New York
- Atkinson A, Selcuk A (2000) Solid State Ion 134:59
- Hendriksen PV, Larsen PH, Mogensen M, Poulsen FW, Wiik K (2000) Catal Today 56:283
- ten Elshof JE, Bouwmeester H MJ, Verweij H (1995) Solid State Ion 81:97
- Mizusaki J, Yoshihiro M, Yamauchi S, Fueki K (1985) J Solid State Chem 58:257
- Kharton VV, Naumovich EN, Nikolaev AV (1996) J Membr Sci 111:149
- Fossdal A, Einarsrud M-A, Grande T (2005) J Eur Ceram Soc 25:927
- Montross CS, Yokokawa H, Dokiya M, Bekessy L (1995) J Am Ceram Soc 78:1869
- Paulik SW, Baskaran S, Armstrong TR (1998) J Mater Sci 33:2397
- Chou Y-S, Stevenson JW, Armstrong TR, Pederson LR (2000) J Am Ceram Soc 83:1457
- Orlovskaya N, Kleveland K, Grande T, Einarsrud M-A (2000) J Eur Ceram Soc 20:51
- Baskaran S, Lewinsohn CA, Chou Y-S, Qian M, Stevenson JW, Armstrong TR (1999) J Mater Sci 34:1
- Kleveland K, Orlovskaya N, Grande T, Moe AMM, Einarsrud M-A, Breder K, Gogotsi G (2001) J Am Ceram Soc 84:2029
- Sammes NM, Ratnaraj R (1995) J Mater Sci 30:4523
- Radovic M, Lara-Curzio E, Riestler L (2004) Mater Sci Eng A368:56
- Chou YS, Kerstetter K, Pederson LR, Williford RE (2001) J Mater Res 16:3545
- Meixner DL, Cutler RA (2002) Solid State Ion 146:273
- Lein HL, Wiik K, Grande T, Solid State Ion. In press
- Faaland S, Vullum PE, Grande T, Holmestad R, Einarsrud M-A (2005) J Am Ceram Soc 88:726
- Ostovoi DY, Gogotsi GA, Suvorov SA, Shevchik AP (2002) Refract Ind Ceram 43:237
- Salje EKH (1990) Phase transitions in ferroelastic and co-elastic crystals. Cambridge University Press, Cambridge
- Kleveland K, Wereszczak A, Kirkland TP, Einarsrud M-A, Grande T (2001) J Am Ceram Soc 84:1822
- Majkic G, Wheeler L, Salma K (2000) Mater Res Soc Symp Proc 575:349
- ISO/CD 15732 Fine Ceramics (Advanced ceramics, Advanced technical ceramics)—Test method for fracture toughness at room temperature by single edge precracked beam (SEPB) method. International Organization for Standardization, Geneva, Switzerland
- Kübler J, Fracture toughness of ceramics using the SEVNB method: from a preliminary study to a standard test method. In: ASTM STP 1409 fracture resistance testing of monolithic and composite brittle materials. ASTM International, West Conshohocken, PA, USA pp 93–106
- Wachtman JB (1996) Mechanical properties of ceramics. Wiley, New York
- Hillig WB (1985) General electric, corporate research and development. No. 85CRD152
- Hillig WB (1986) Mater Sci Res 20:697
- Hillig WS (1993) J Am Ceram Soc 76:129
- Moruzzi VL, Shafer MW (1960) J Am Ceram Soc 43:367
- Fossdal A, Einarsrud M-A, Grande T (2004) J Solid State Chem 177:2933
- Batti P (1962) Ann Chim (Rome) 52:941
- Fett T, Munz D, Thun G (1998) J Am Ceram Soc 81:269
- Fett T, Munz D, Thun G (2003) J Eur Ceram Soc 23:195
- Atkinson A, Ramos TMGM (2000) Solid State Ion 129:259